processes

MDPI

Article

Coffee-Waste-Based $ZnCl_2$ Activated Carbon in High-Performance Supercapacitor Electrodes: Impact of Graphitization, Surface Morphology, Porosity and Conductivity

Sami Mukhiemer [1], Allan Daraghmah [1,*], Heba Nassar [2], Shahzad Hussain [3], Hanyi Lim [4], Hyobin Han [4], Tae Woo Kim [4], Ameed N. Amireh [2] and Hikmat S. Hilal [2,*]

[1] Department of Physics, An-Najah National University, Nablus P400, Palestine; s.mkhimar@najah.edu
[2] Department of Chemistry, An-Najah National University, Nablus P400, Palestine; h.nassar@najah.edu (H.N.); ameed.amireh@najah.edu (A.N.A.)
[3] Department of Engineering, University of Cambridge, Trumpington St., Cambridge CB2 1PZ, UK; sh2202@cam.ac.uk
[4] Hydrogen Research Department, Korea Institute of Energy Research, 152, Gajeong-ro, Yuseong-gu, Daejeon 34129, Republic of Korea; giant0113@naver.com (H.L.); hyobin@kier.re.kr (H.H.); twkim2015@kier.re.kr (T.W.K.)
* Correspondence: authors: allan.d@najah.edu (A.D.); hshilal@najah.edu (H.S.H.)

Abstract: Activated carbon (AC) electrodes from coffee waste (CW) were earlier assessed in supercapacitors but showed lower supercapacitor performance in terms of specific capacity (C_s), specific power (P_s) or both, compared to other biowastes. This work describes how CW-based AC electrode performance may be improved if carefully prepared. Careful processing yields higher graphitization, carbon content (aromaticity), conductivity and porosity free of any residues. Thus, AC electrodes will exhibit higher C_s and P_s simultaneously. CW was first pyrolyzed (C_{Pyrol}) and then chemically activated by $ZnCl_2$ (AC_{Chem}). Both materials were characterized using SEM, TEM, BET, FT-IR spectra, Raman spectra and XRD. The AC_{Chem} exhibited much higher graphitization, crystallinity, specific surface area (*SSA*), porosity and conductivity. From cyclic voltammetry, the AC_{Chem} electrode exhibited a C_s of 261 F/g, an energy density of 18.3 Wh/kg and a P_s of 360 W/kg at 0.33 A/g. From galvanostatic charge–discharge, there was a stable C_s of 150 F/g at 0.33 A/g over 5000 charge–discharge cycles. From electrochemical impedance spectroscopy, the *Cs* was ~180 F/g, with a low equivalent series resistance (*ESR*) of 0.56 Ω at a frequency of 0.01 Hz, compared to the literature. The AC_{Chem} electrode was superior to the C_{Pyrol} electrode and to earlier CW-based AC counterparts, with much lower resistance. Moreover, the electrode competed with other biowaste-based electrodes.

Keywords: porous and conductor coffee waste-based carbon; highly graphitized AC; $ZnCl_2$ supercapacitor electrode; specific capacitance; specific power

Citation: Mukhiemer, S.; Daraghmah, A.; Nassar, H.; Hussain, S.; Lim, H.; Han, H.; Kim, T.W.; Amireh, A.N.; Hilal, H.S. Coffee-Waste-Based $ZnCl_2$ Activated Carbon in High-Performance Supercapacitor Electrodes: Impact of Graphitization, Surface Morphology, Porosity and Conductivity. *Processes* **2024**, *12*, 2832. https://doi.org/10.3390/pr12122832

Academic Editor: Mingxia Gao

Received: 13 November 2024
Revised: 2 December 2024
Accepted: 6 December 2024
Published: 10 December 2024

1. Introduction

Many reasons stand behind considering biowastes as sources of carbon materials in modern devices. Firstly, recycling biowastes prevents widespread environmental contamination from random dumping. Secondly, the produced carbon is useful as a low-cost and safe material for electronic devices. Thirdly, the strategy minimizes dependence on the hazardous fossil sources [1–3]. A promising application area is supercapacitor (SC) technology for energy storage. The SC is a device with two high specific surface area (SSA) electrodes, a separator and an electrolyte solution. Compared to conventional capacitors, SCs have much higher capacitance [4–7]. With potentially high power yields, SCs are

considered in various electronic devices, and specifically electric cars, competitively with batteries [5,8].

The Ragone plots describe how SCs are at intermediary positions between conventional capacitors and batteries [9]. The plots combine energy density with power density outputs for various energy-storage devices, including fuel cells, batteries and SCs, together with conventional capacitors. For a given device, lowering the equivalent series resistance (*ESR*) increases the energy density, while raising the voltage window increases the power density values [9–11].

Improved energy-density storage devices are continuously needed to meet expanding demands for modern electronic devices. As in batteries, electrochemical capacitors (ECs) attract special attention by virtue of their high storage density, low-temperature performance and multiple charge–discharge cycles. Unlike batteries and fuel cells, SCs involve no real chemical reactions and function for prolonged life cycles [12], which is one virtue. SCs with both high energy density (like batteries) and high power density (like capacitors) at the same time are highly needed. SC research is thus active in achieving this feature.

In SCs, very high specific surface area (SSA) electrodes with high conductivity are necessary. The need for carbon materials in SCs is thus justified. Activated carbons (ACs) are conducting materials that are thermally and chemically stable and can have large SSAs with high micropore volumes. With high adsorption capacity and tunable pore structures [13], ACs are being considered in various energy-storage devices such as supercapacitors [14,15].

AC characteristics (surface, pore structure and adsorption capacity) are affected by preparation and activation methods. Two types of activation are widely known: physical activation and chemical activation. In chemical activation, impregnation with a suitable material is used. Examples of widely used chemical activating agents are KOH, NaOH, K_2CO_3, $ZnCl_2$ or H_3PO_4. The activating agents, which are used in combination with mild physical processing, ensure pyrolytic decomposition of the precursor material at lower processing temperatures, with less tar formation [16,17]. In physical activation, the precursor material is partially gasified under inert atmospheres at a high temperature and then activated with oxidizing gases such as steam, air, carbon dioxide or mixed gases [17].

Chemical activation is a simple process and is advantageous in terms of processing time, low temperature and high yield with high porosity. However, physical activation is still preferable on a commercial scale due to the higher control of characteristics and simplicity [18].

High-temperature pyrolysis can be coupled with poro-genic processes using NaOH or KOH activation. Hazelnut shell hydrothermal carbonization (HTC) was studied by three various poro-genic methods, namely simple heat treatment, KOH activation and MgO templating. Better electrochemical characteristics (with higher SSA and effective micro-porosity) were reported in anode materials for energy storage [18,19]. Ginkgo waste-based ACs, activated by KOH, were reported by Jiang et al. [20]. The effect of pre-carbonized stuff and the KOH ratio was studied. SSA values of 1829.7 m^2/g were observed for samples activated with KOH. The AC showed a specific capacitance (C_s) of 365 F/g at a scan rate of 2 mV/s. KOH was also used as an activating agent at 600–900 °C for 2 h and yielded N-doped AC with a large SSA of 3401 m^2/g, a high C_s of 346 F/g and a high-capacity stability (~98% for 5000 cycles at 1 A/g), but a low energy density of 22.4 Wh/kg (at 0.5 A/g) [21].

Chestnut shell-based AC, activated with $ZnCl_2$, exhibited an SSA of up to 1987 m^2/g with a C_s 105.4 F/g [22]. Hong et al. used K_2SO_4 to activate chestnut shell-based AC with an SSA of 1412 m^2/g and a C_s of 265 F/g, but at a low current density (0.1 A/g) [21].

$KHCO_3$ was described as activating AC from chestnut shells for supercapacitor electrodes [21]. Biochar activation with $KHCO_3$ yielded porous carbons with a high SSA of 2298 m^2/g and a C_s of 387 F/g (at 2 A/g) with high stability (~99% after 10,000 cycles at 30 A/g) [21,23]. N-doped porous carbon from edible Chinese water-chestnut corms was also

reported [22]. Melamine also activated chestnut shell-based carbons [23]. The AC exhibited current density (0.5 A/g), C_s (402.8 F/g) and SSA (691.8 m^2/g). The literature thus showed the possibility of producing chemically activated carbons for high-performance supercapacitors from various biowastes. Depending on their regional agricultural resources and biowastes, researchers tend to focus their study attention. For this reason, in many regions, people have conducted their studies on chestnuts, hazelnuts and other nuts.

Other sources are globally spread, such as coffee wastes (CWs), since coffee is widely used in many places. It is reported that in the early 2020s, more than 5 million tons of coffee was globally consumed [24]. More recently, the amounts of CW were reported to exceed 8 million tons [25]. ACs with high surface areas and pore volumes from CW were prepared and used for contaminant removal by adsorption [24,26–28].

CWs thus deserve to be studied. CW-based electrodes were reported in supercapacitors. A flexible supercapacitor with a C_s value of 139 F/g (at 0.5 A/g), a specific energy of 12.5 W h/kg and a specific power (P_s) of 202 W/kg was prepared from nitrogen 8%-doped AC. The KOH activation was conducted at various temperatures. The supercapacitor functioned for more than 5000 cycles with ~90% capacitance retention [29]. However, the results showed lower C_s values than ACs from other waste materials. Electrochemical impedance spectroscopy (EIS) showed high resistance (*ESR*) values as well. Chiu et al. prepared AC in one combined process (physical and chemical activations) with various activating agents, KOH being the best. Only a relatively low C_s of 105.3 F/g was observed [30]. M Biegun et al. used hydrothermal acidic hydrolysis, then the KOH activation at 800 °C, to activate coffee waste and obtained a high SSA of ~2900 m^2/g. Using a liquid ionic electrolyte, the highest C_s was 178 F/g at 50 A/g, based on the galvanostatic charge–discharge (GCD) method [31], still with lower performance than other waste-based materials described above. Omkar Khadka et al. recently prepared supercapacitor electrodes from coffee wastes, first by chemical activation with a $ZnCl_2$ 1:1 ratio, then by physical activation at 700 °C, and observed a relatively low C_s of only 113.8 F/g at 1 A/g [32]. In a recent review, Davidraj et al. reported the possibility of food waste materials to produce electrodes for energy-storage devices [33]. The report cited a number of papers using CWs in supercapacitor electrodes. In another more recent review, Pagett et al. described CWs in supercapacitor electrodes [25]. With the exception of one 2008 report that showed high C_s [34], all other more recent reports showed C_s values of less than 160 F/g [25]. From the literature, it can be noted that the AC prepared from coffee wastes showed lower performance than other ACs prepared from other sources, as summarized in Table 1.

Table 1. Some literature reported performance values for electrodes from biowastes.

Waste Source	Spec. Capac. (F/g)	Spec. Energy W h/kg	Spec. Power (W/kg)	*ESR* (Ω)	Ref.
CW	139 (0.5 A/g)	12.5	202	~50	[29]
CW (with ionic liquid)	178 (at 50 A/g)	84	202	0.20	[31]
CW KOH	105-21	6.9	350	--	[30]
CW	113 (1 A/g)	--	--	--	[32]
CW	<160				[25]
Chestnut	265 (0.1 A)	--	--	--	[21]
Chestnut	~403	26	454.5	--	[23]
Ginkgo	365 (scan rate 2 mV/s)	--	--	0.2	[20]
Oak seeds	551 (1 A/g)	18.5	14900	1	[35]
Date waste	179 (scan rate 5 mV/s)	--	--	10	[36]

Instead of using the highly corrosive KOH activating agent reported earlier, the environmentally friendly and low-cost $ZnCl_2$ is used here. The choice for $ZnCl_2$ is based on its eco-friendliness, acidic nature and high performance, as described earlier [37], where it yielded ACs with high surface areas and high adsorption capacity. $ZnCl_2$ was described in activating coffee waste for supercapacitor electrodes with a C_s of 134 F/g at 1 A/g using organic solvents, with high equivalent series resistance (*ESR*) of more than 20 Ω [38]. In a recent study [39], $ZnCl_2$ was described in CW-based activated carbon (AC). Based on cyclic voltammetry, the AC showed a high *Cs* of 250 F/g but at a low scan rate of 1 mV/s. At a scan rate of 5 mV/s, the *Cs* value was lowered to ~195 F/g, which means the electrode still needs further improvement. From charge–discharge, the study also showed a high *Cs* value of ~200 F/g at a current density of 1 A cm^{-2}. However, the study did not show the results of electrochemical impedance spectroscopy (EIS) and thus did not display the *ESR* values that are important in P_s determination.

In CW-based ACs, no correlation between important characteristics (such as surface area, porosity, graphitization and morphology) with electrode C_s and P_s was reported. As CW is a promising source of AC, more studies are needed to increase the CW-based supercapacitor performance. In supercapacitor electrode technology, high values of both C_s and P_s are necessary. Both features can be improved by tailoring the properties of the electrode material at its microscale. For instance, to achieve high C_s, the electrode material must have high *SSA* and porosity. High total pore volume, especially at the microscale, is necessary to uptake higher charges. Moreover, the electrode must exhibit relatively high conductivity to be able to conduct current at the AC/metal collector interface in order to exhibit a high P_s. To achieve this, the AC electrode material must have a higher carbon content (carbon purity) with high aromaticity. By virtue of C=C conjugated bonds, in the aromatic AC framework, the electrode may conduct current. Therefore, AC electrodes with higher carbon content and crystallinity are necessary to achieve these characteristics.

On the other hand, the pore availability to charges is very critical in superconductor electrodes. Therefore, special attention should be paid to removing all traces of organic materials and residues, even before chemical activation, to guarantee that the resulting ACs have more open pore structures.

All these assumptions will be tested. The goal here is three-fold: First, to produce AC electrodes from CW with high *SSA* and micro-porosity that are free of any residues of organic stuff and have a high C_s. Second, to produce highly graphitized AC electrodes with high carbon content, aromaticity and conductivity in order to exhibit high P_s values. Again, the AC must be free of any organic residues to improve interparticle charge transfer for increased conductivity. Third, to correlate between AC electrode C_s and P_s (measured from galvanostatic charge–discharge, cyclic voltammetry and electrochemical impedance spectra) with AC material and other characteristics. *SSA* and porosity will be examined using the BET method.

Crystallinity will be examined using X-ray crystallography. Morphology will be studied using scanning electronic microscopy. Graphitization, carbon content and purity, functional groups and aromaticity will be examined by Raman spectra, FT-IR spectra and energy dispersive X-ray electron spectra. The study will be performed on an AC electrode in comparison with another counterpart prepared from CW pyrolysis.

Extra steps will be followed in preparing the pyrolyzed carbon and the AC materials, as described in Experimental Section 2. The impact of these steps on the AC characteristics and supercapacitor performance will be assessed here by comparison with the literature electrodes in Section 3.

This comprehensive study approach to CW carbon materials was not reported, to our knowledge. The present study thus aims to produce an AC electrode from CW with higher C_s, higher P_s and lower *ESR* than earlier described systems.

2. Experimental

2.1. Materials

Organic solvents, such as acetone, bases and acids, were purchased from Sigma-Aldrich (St. Louis, MO, USA) in pure forms. The glass fiber separator (-M 5V5) was purchased from Alter-Lab. Coffee waste was taken from freshly used Turkish coffee drinks (*Arabica* type). The coffee beans were brown roasted at ~240 °C for ~20 min. The roasted beans were then ground on a Ditting shop grinder at super-grade 0.1 mm in diameter. The coffee drink was then processed according to Turkish coffee drink protocols and boiled for a few minutes. The resulting CW was isolated and stored in a refrigerator for processing.

2.2. Equipment

A hydraulic press (Shimadzu), equipped with a pressure gauge, was used to make AC disks. The sample was pressed at 7 tons. The value was based on earlier recommendations [37].

A standard Teflon Swagelok cell, 10 mm in diameter with stainless steel electrodes, was used for supercapacitor testing. The cell was connected to the potentiostat/galvanostat (VoltaLabPGZ402). The working electrode was connected to one side, while the counter and the reference electrodes were together connected to the other side. The internal reference cell was used as a reference. The VoltaMaster 4 software was used for electrochemical measurements. Solid-state Fourier transform infra-red spectra were measured on a Thermo Fisher (Waltham, MA, USA) machine (ASB1200315-Nicolet 5 FT-IR Spectrometer).

AC morphology and surface structure were examined by scanning electron microscopy (SEM) on a (Hitachi-S-4800 Field-Emission machine). Transmission Electron Microscopy (TEM) was measured on a JEM-ARM200F system. Brunauer–Emmett–Teller (BET) was measured on Micromeritics-3Flex 3500 equipment. X-ray diffraction patterns were measured on a PAN-alyticalX'Pert-PRO X-ray diffractometer, using Cu Kα as a source. Raman spectra were measured on OlympusBX41M equipment. SEM, XRD, TEM, BET, XPS and Raman spectra were all measured in the labs of the KIER, Daejeon, Korea.

2.3. Carbon Material Preparation

The CW material described above was treated by two methods, namely pyrolysis only and chemical activation.

- ***Thermal (pyrolytic) treatment (C_{Pyrol})***

Pre-dried *Arabic* coffee waste (200 g) was soaked in distilled water (800 mL) for 24 h and rinsed. The solid was again soaked in hot distilled water (800 mL) for 24 h, filtered, rinsed with ethanol, spread on a tray and dried in an oven at 200 °C for 3 h, then left at 50 °C for 24 h. The remaining solid waste was left to dry at room temperature for 24 h, then heated in an oven at 70 °C for 12 h. The extra steps were performed to remove all soluble coffee ingredients, including any possible organic oils or residues.

The resulting solid was then heated at 800 °C for 2 h under a flow of inert ultrapure N_2. The solid was kept to cool in the oven for 24 under N_2. The resulting C_{Pyrol} was stored inside a desiccator. The net mass for the C_{Pyrol} was ~154 g, with a yield percent of 77%.

- ***Chemical activation (AC_{Chem})***

A C_{Pyrol} sample (100 g) was taken and magnetically stirred with $ZnCl_2$(s) (in a 1:1 mass ratio) for 24 h at 60 °C. The solid mixture was left at room temperature for 24 h and then oven-dried for 7 h at 70 °C. The solid mixture was heated at 800 °C for 2 h. The resulting solid was cooled and soaked again in water for 24 h to remove any floating materials. The solid was then filtered, rinsed with water and dried at room temperature for 48 h. The resulting AC_{Chem} was stored in a desiccator for further use. The net mass for AC_{Chem} was

~78 g, with a yield of 78%. In both cases, no ash was observed, indicating that gasification was the main reason for the loss.

2.4. Carbon Disc Electrode Preparation

A sample from each carbon was ball-milled to fine powder with Agat mortar for 10 min. The carbon material was mixed with PVDF polymer in a 93:7% ratio and was magnetically stirred with acetone (15 mL) to allow polymer diffusion inside the carbon. The mixture, which became fluidic muddy, was then sonicated at 35 °C for 20 min inside a bath and then left at room temperature for 24 h to evaporate off the acetone. The resulting solid/polymer cake (with polymer in and out) was milled with a mortar to a fine powder. The excessive polymer tissue, which resulted on the sides, was peeled off with a tongue. The remaining solid was collected and oven-dried at 70 °C for 2 h. The carbon powder (0.03 g) was then used to make electrode discs, which were pressed in a mold under hydraulic pressure of 7 tons. The carbon disc diameter was 10 mm, and the disc thickness was ~0.19 mm.

2.5. Electrochemical Methods

Electrochemical characteristics for both carbon materials were examined by various methods, namely galvanostatic charge–discharge (GCD), cyclic voltammetry (CV) and electrochemical impedance spectroscopy (EIS). A Swagelok cell, described above, was used in the electrochemical studies. One disc was loaded as a coating layer on one stainless steel electrode. A fiberglass disk separator (with a diameter of 10 mm) was immersed in KOH electrolytic solution (6 M) for 5 min and was then carefully taken by tongues and firmly stacked on the carbon electrode as a coating. The other carbon disc was stacked onto the separator. Then, the cell was firmly assembled to prevent gaps and bubbles between electrodes and to disallow any cell component movements. The assembled Swagelok cell electrodes were connected with the PGZ 402 Potentiostat/Galvanostat in the two-terminal mode, as described above. The VoltaMaster 4 software was utilized in data collection. The CV measurements were performed for each electrode in the potential range of 0.0–1.0 V at various scan rates.

The GCD data were measured at various current densities. The current density was switched between positive values (for charging) and negative values (for discharging). The results were acquired and analyzed using Origin software (Version 4.0.9.0 – November 13th, 2023) or Excel (2010).

3. Results

3.1. Carbon Disc Characterization

- ***Carbon Morphology***

Figure 1 shows SEM micrographs for both carbon materials in pressed disc forms. The C_{Pyrol} and AC_{Chem} materials exhibited different surface morphologies. The AC_{Chem} is more porous than the C_{Pyrol}. This is due to the chemical activation, which further affects the carbon surface, in addition to heating, as reported earlier [40,41]. As stated above, the acidic $ZnCl_2$ activating agent interacts with the carbon matrix and makes it more porous.

In Figure 2, TEM micrographs for both carbon materials are shown. In each case, white dots can be observed, indicating pores. The AC_{Chem} was more porous, with higher homogeneity, than C_{Pyrol}. A closer look at Figure 2c shows that the AC_{Chem} involves planes similar to graphene, which are normally planes present in graphite. The interplanar distances are ~0.334 nm, which resembles the earlier literature [42]. This indicates that AC_{Chem} has high graphitization and carbon purity, as confirmed by other methods as described below.

- ***Carbon material porosity***

The porosity for the two carbon materials was measured using the BET method. Porosity involves SSAs, pore size distributions (PSDs) and total specific pore volumes. Adsorption/desorption isotherms were measured for both carbon materials in pressed disc forms. The results are summarized in Figure 3a. The figure indicates that at higher relative pressure, the amount of gas that entered the pores increased until all pores were occupied at equilibrium. Naturally, the equilibrium position was pushed to higher adsorption at higher relative pressures.

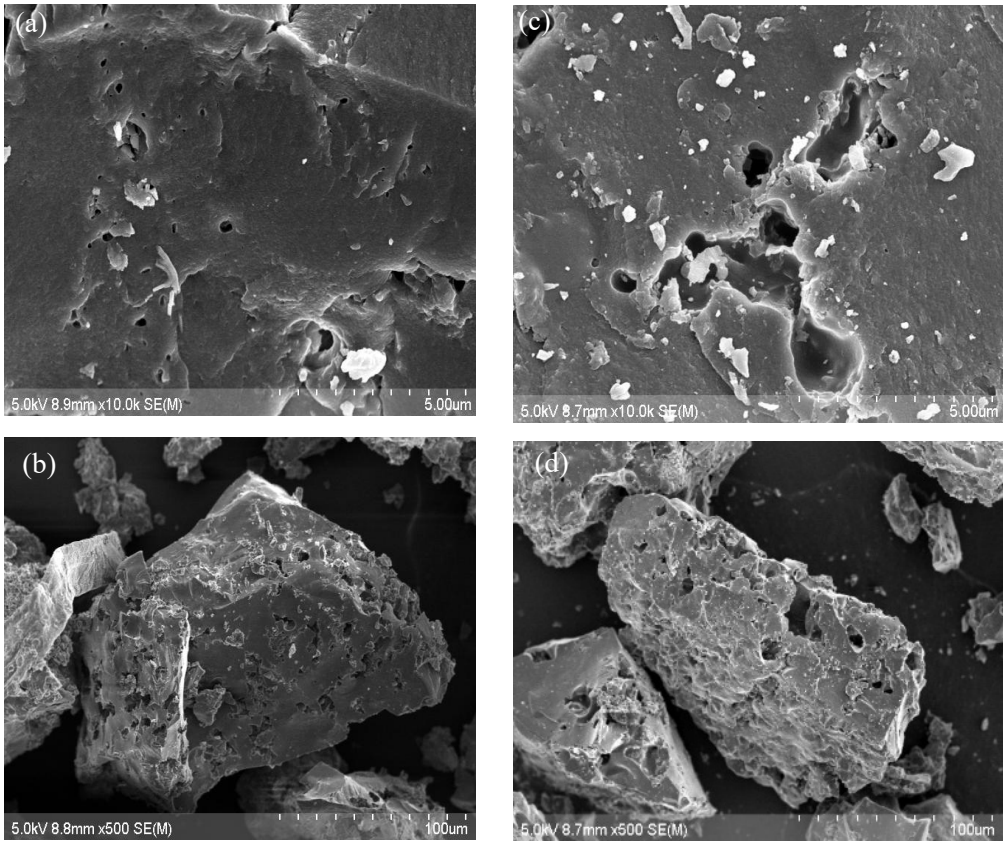

Figure 1. SEM micrographs measured for coffee waste-based carbons as pressed discs. (**a**,**b**) For C_{Pyrol}; (**c**,**d**) for $AC_{Chem.}$

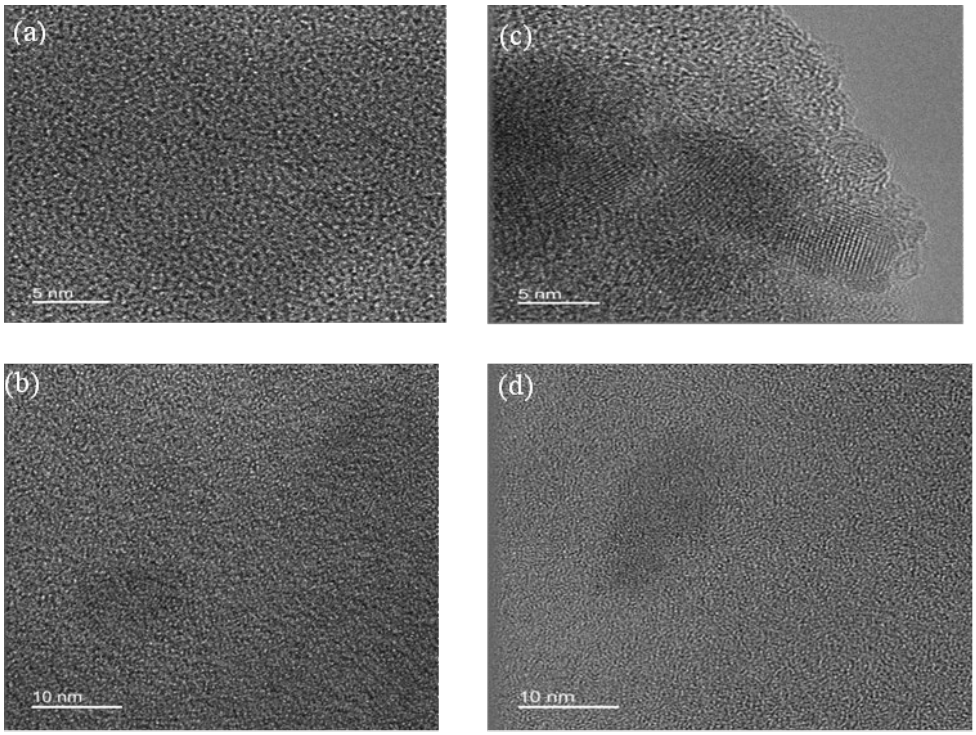

Figure 2. TEM micrographs measured coffee waste-based carbons as pressed discs. (**a**,**b**) For C_{Pyrol}; (**c**,**d**) for AC_{Chem}.

To understand the effect of electrode material pore size distribution on the C_s, BET analyses were performed (Figure 3a). The isotherms involved small hysteresis loops from high to low pressure ranges. This indicated that the electrodes had both meso- and macroporosities. Based on IUPAC, the present isotherms are type I [43]. This indicates highly microporous materials. AC_{Chem} exhibited higher nitrogen adsorption, even at very low relative pressures ($P/P° < 0.01$), compared to C_{Pyrol}. This indicated the existence of micropores, more profoundly in the former than in the latter. The AC_{Chem} is superior to C_{Pyol} in terms of *SSA*, in addition to micro-porosity, as described in Table 2. As the minimal pore sizes for AC_{Chem} (0.8 nm) and C_{Pyrol} (1.8 nm) are larger than the ionic sizes for both electrolyte ions ($K^{+}_{(hydrated)}$ 0.4 nm, $OH^{-}_{(hydrated)}$ 0.38 nm), both activated carbons readily adsorb the ions and may behave as supercapacitors. Since the AC_{Chem} had more total micropores than C_{Pyrol}, with higher *SSA (vide infra)*, the former carbon should have higher C_s.

The *SSA* was determined by multiple point BET approach within regions of isotherms, limited by the P/P^{o} range of 0.0–0.3. Figure 3b summarizes the results. The adsorption volume showed that BET surface areas for C_{Pyrol} and AC_{Chem} were 458 and 830 m^2/g, respectively. The total volume of pores (V_{total}, cm^3/g) was calculated by the amount of adsorbed nitrogen at $P/P° \approx 0.9932$. All results are summarized in Table 2.

Table 2. BET data measured for C_{Pyrol} and $AC_{Chem.}$

	BET-Based Data							
Material	S_{BET} (m^2/g)	V_t[b] (cm^3/g)	$V_{0.5–2}$[c] mic (cm^3/g) t-plot	$V_{2–5}$[e] (cm^3/g) BJH Meso	$V > 50$ (cm^3/g)	S_{mic} (m^2/g)	S_{meso} (m^2/g)	*APS* (nm)
C_{Pyrol}	458	0.2114	0.153	0.23	0.0084	385	73	1.8–3.3
AC_{Chem}	830	0.41	0.19	0.072	0.148	755	75	1.0–4.0

S_{BET} = BET-based *SSA*, S_{mic} = micropore surface area, S_{meso} = mesopore surface area, V_t = total pore volumes, V_{mic} = micropore volume, V_{meso} = mesopore volume, *APS* is pore size (nm).

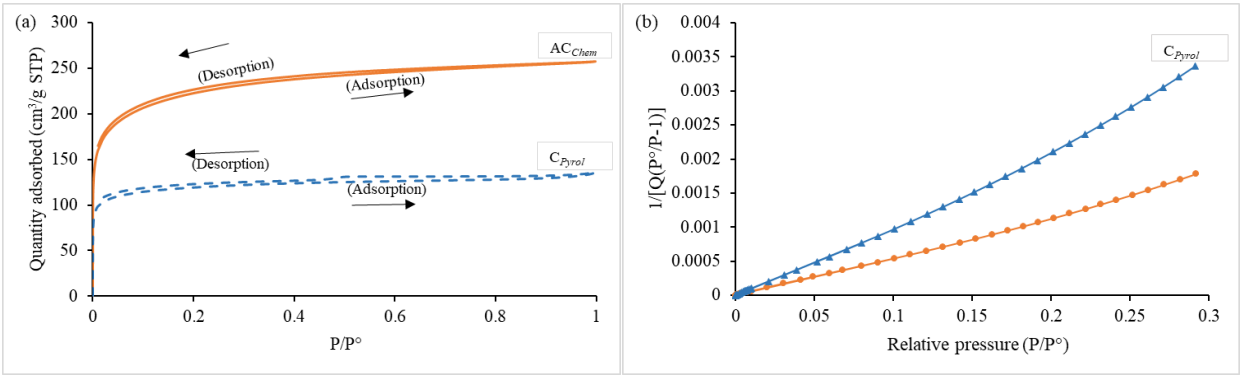

Figure 3. BET results for AC_{Chem} and C_{Pyrol}. (**a**) Adsorption isotherms and (**b**) 1/[Q(P°/P − 1)] vs. P/P° plots.

All the above results confirmed the AC_{Chem} high porosity and suitability for supercapacitor applications. The increased porosity is due to using the activating agent.

- ***Pore size distribution by the BJH method***

The method of Brunauer–Joyner–Halenda (BJH) method was used to analyze meso- and macro-pores in a wide diameter range of 17–3000 Å. Figure 4a summarizes the pore size distributions in both carbons. The pore size distributions were in the micro-, meso- and macropore scales. The figure shows that for the present electrodes, the domain of pore sizes was centered in the ranges of (1.8–3.3 nm) for C_{Pyrol} and (0.8–2.7 nm) for AC_{Chem}. Equation (1) describes the relation between BET surface area and pore size with C_s.

$$C_s = \varepsilon A/d \quad (1)$$

where ε is electrolyte dielectric constant, A is SSA accessible to ions and d is spacing between ions and electrode-pore surface (in nm).

Based on this equation, two methods can be followed to increase supercapacitor charge storage:

- Improving *SSA;*
- Decreasing spacing between electrode surface and ions.

Therefore, higher *SSAs* and higher meso- and micropores numbers, together, yield higher transport of charges. This consequently leads to higher C_s.

The results showed that, for both present carbons, higher adsorbed gas occurred in the smaller pore size. Small pore sizes were more dominant in the AC_{Chem}, as observed from pore size distributions (differential pore volumes) (Figure 4a). The observed AC_{Chem} material peaks were distributed within the pore size range of 1.0–4.0 nm. Thus, micropores were dominant in the AC_{Chem}, with higher adsorption at smaller diameter micropores. The results justified the high C_s for AC_{Chem}, as summarized in Table 2.

As per C_{Pyrol}, the plot showed a single peak at 3.7 nm. At smaller pore sizes, C_{Pyrol} has lower adsorption than the AC_{Chem}. The results clearly indicated that the AC_{Chem} was more microporous than the other counterpart.

- ***Pore size distribution by the (HJ) t-plot***

The micropore volume and surface area (S_{micro}, m^2/g) were investigated by the Harkins–Jurat plot. The amount of adsorbed N_2 for a given P/P° range was plotted against pore thickness (t). The results are summarized in Figure 4b,c and Table 2. From the figures, the present electrodes involved high micro-surface areas of 557 and 385 m^2/g for AC_{Chem} and C_{Pyrol} electrodes, respectively. This justified the high C_s for AC_{Chem}, as described below.

- ***X-ray patterns***

The XRD pattern is presented in Figure 5a. Both C_{Pyrol} and AC_{Chem} exhibited a peak at 2Θ = ~24°. This is consistent with the earlier literature [41]. However, as both materials are amorphous, broad and low diffraction peaks for the (002) signals were observed. The peak

for AC_{Chem} was sharper than for C_{Pyrol}, which indicated that the former was more crystalline. This means that the former had more carbon content than the latter, as described below. The especially broad peak for the C_{Pyrol} is a result of the presence of additional phases, as described in the literature [42]. The XRD pattern occurred at a slightly lower 2Θ value by adding KOH to activated carbon from oil palm fruits [43]. In the present study, no clear shifting is observed due to overlap.

Another broad peak in the range of 2Θ = 40–50° can also be observed more obviously for AC_{Chem} than for C_{Pyrol}. The AC_{Chem} thus showed more resemblance to earlier chemically activated carbons [44]. The XRD patterns indicated that the AC_{Chem} had higher graphitization, crystallinity and porosity.

- ***Elemental analysis***

For both C_{Pyrol} and AC_{Chem}, elemental analyses were performed by the *EDS*, as described in Supplementary Figures S1a,b. Table 3 summarizes the results.

Table 3. Summary of elemental analysis results for (a) AC_{Chem} and (b) for C_{Pyrol}.

	Element	C	N	O	S	Cl	Fe
a	Atom%	93.3	2.3	3.9	0.1	0.2	1×10^{-2}
	Mass%	96.6	0.3		0.1	0.2	2×10^{-2}
	Element	C	N	O	S	Cl	Fe
b	Atom%	63.2	1.9	23.7	0.04	1.1	0.04
	Mass%	83.3	4.0		0.1	1.5	0.1

For AC_{Chem}, the atom percentage for carbon was 93%, while for C_{Pyrol}, it was only 63.20%. So, more carbon appears in AC_{Chem}, which is a virtue for this material. The results are also consistent with TEM results where the AC_{Chem} involves graphene planes in the graphite. The EDS results were also consistent with the XRD results, in the sense that AC_{Chem} material had higher graphitization; *vide infra*.

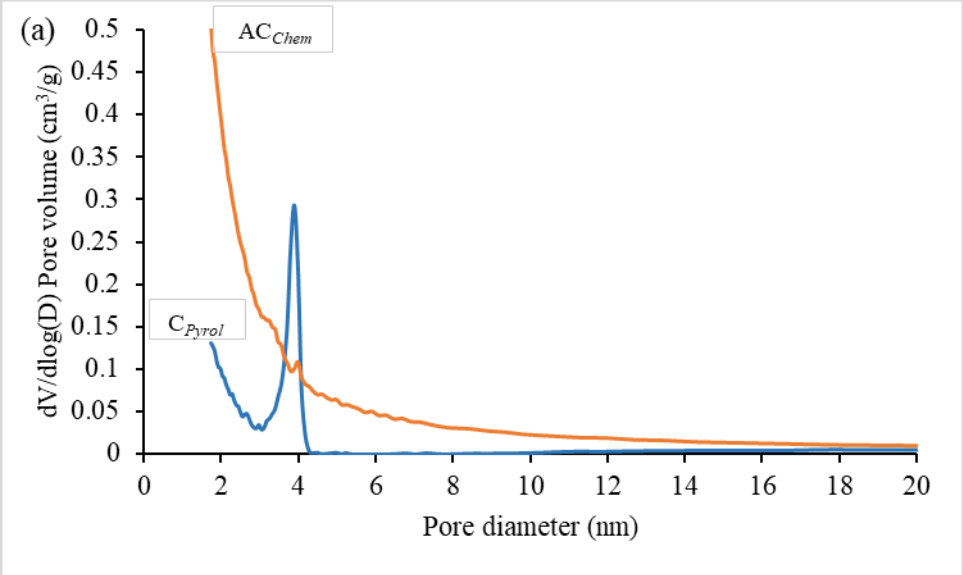

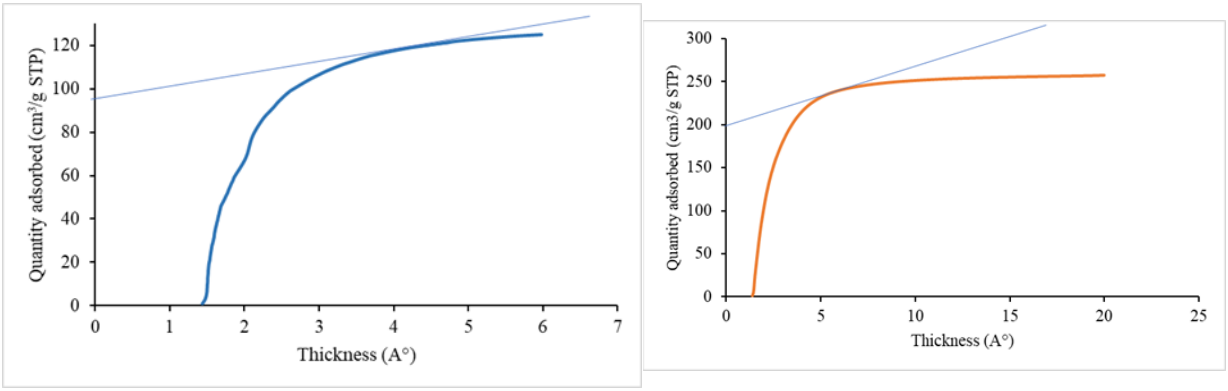

(**b**) (**c**)

Figure 4. Pore size distribution based on BJH method. For C_{Pyrol} and AC_{Chem} activated carbons. (**a**) Plots of pore volume vs. pore size. Plots of quantity adsorbed vs. thickness for (**b**) C_{Pyrol} and (**c**) AC_{Chem}.

- ***FT-IR spectra:***

Solid-state FT-IR spectra were measured for both carbon materials, as described in Figure 5b. Both carbon materials are free of significant water amounts, as both did not show strong characteristic bands at ~3500 cm^{-1}. This also indicated the absence of the O-H bonds that exhibit a broad band due to H-bonding when the groups are in close proximity. C_{Pyrol} showed a clear band at ~2900 cm^{-1} due to C-H bond stretching in (-CH_2) and in (-CH_3) groups [44,45]. The same band was not clearly observed in AC_{Chem}, which indicated low H-content in the solid, as earlier reported for dry graphite [46,47]. The results indicated that the AC_{Chem} had less hydrogen and more carbon than C_{Pyrol}. Naturally, AC_{Chem} had higher graphization and carbon purity with a higher chance of C=C formation than its counterpart. This was further evidenced by the -C=C- band at ~1600 cm^{-1}, typical for aromatic systems [48], being clearer and stronger in AC_{Chem}. Moreover, the ~1700 cm^{-1} band, associated with the C=O bond in ketones, aldehydes and carboxylic acids [45], was clearly observed in C_{Pyrol} but not in AC_{Chem}.

The FT-IR spectra therefore confirmed the higher graphitization and carbon purity in AC_{Chem} compared to the C_{Pyrol} counterpart. With higher graphitization, the carbon material was able to assume a more aromatic structure, carbon purity and higher conductivity, in congruence with the elemental analysis in Table 3. These results were further corroborated by the Raman spectra described below.

- ***Raman spectra***

Figure 5c below summarizes the Raman spectra for C_{Pyrol} and $AC_{Chem.}$ The AC_{Chem} exhibited higher homogeneity than C_{Pyrol}. Each carbon material exhibited two sharp peaks at 1360 cm^{-1} (for the D peak) and 1590 (for the G peak). Comparison between the two spectra indicated that the ratio between the D-peak intensity (I_D) and the G-peak intensity (I_G) was 0.7 for AC_{Chem} compared to 0.8 for C_{Pyrol}. A lower I_D/I_G ratio means higher graphitization in carbon materials, as described earlier [49,50]. Therefore, the AC_{Chem} here had more graphitization and carbon purity than the C_{Pyrol}. This result corroborated the XRD and EDS results discussed above in the sense that the former has more C content than the latter. The Raman spectra also corroborated the FT-IR spectral findings discussed above.

It should be noted that higher graphitization is a favored feature in ACs. Researchers tend to increase graphitization by increasing temperature [51]. To increase carbon content with higher *SSA*, porosity and larger total pore volume, chemical activators are needed [52,53].

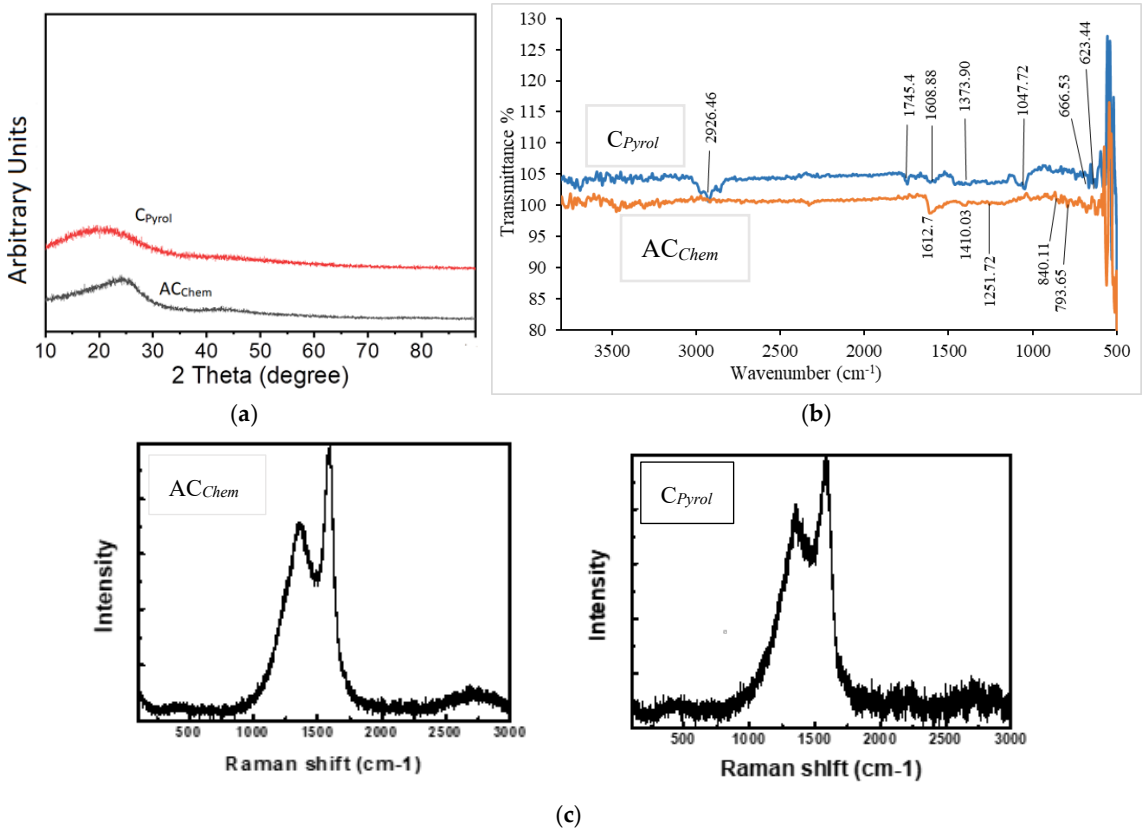

Figure 5. Characterization results for AC_{Chem} and C_{Pyrol} by (**a**) XRD, (**b**) FT-IR spectra and (**c**) Raman spectra.

3.2. Supercapacitor Testing

As described above, the AC_{Chem} electrode was singled out for further in-depth electrochemical study unless otherwise stated. It is customary to single out ACs produced with activating agents in electrochemical studies [30,54]. However, for the C_{Pyrol}, the electrochemical results are displayed in the Supplementary Data, Figures S2–S4, for comparison purposes. Electrochemical results for AC_{Chem}, including CV, GCD and EIS, are described here, using KOH (6.0 M) as an electrolyte.

- ***CV***

CV is a major tool for studying C_s. Cyclic voltammograms were measured in the range (0.0 to 1.0 V) at various scan rates (5, 10, 20, 50 and 100 mV/s) for the AC_{Chem} electrode (Figure 6). Figure 6a displays CVs measured at different scan rates, while Figure 6b displays CVs at one low scan rate (5 mV/s) only. Each CV plot exhibited a semi-rectangular shape, with no peaks and with a highly reversible charge–discharge process. The electrode thus behaved as an electronic double-layer capacitor [4,8,55–57]. The C_s values (in F/g) were calculated from CV plots using Equation (2).

$$C_s = \frac{2x(q_a + |q_c|)}{m\Delta V} \quad (2)$$

where m is the electrode-active material (g) and ΔV is the voltage window (V), while q_a is the anodic charge and q_c is the cathodic charge (in C).

High reversibility for AC_{Chem} electrodes at different scan rates and high response (in charging/discharging) were due to high conductivity, as described in other systems [58–60]. Based on Figure 6a,b, the C_s values for AC_{Chem} were plotted vs. scan rates. Figure 6c indicated that C_s decreased at higher scan rates. Table 4 summarizes the results. The table shows that the present AC_{Chem} electrode was superior to earlier coffee waste-based electrodes in terms of C_s value.

Typically, high C_s is associated with lower scan rates. In AC_{Chem}, the same behavior was observed due to enough time available for ions to penetrate through micropores (of less than 2 nm). At higher scan rate settings, only larger pores (2–50 nm) can uptake ions and contribute to capacitance. That is due to electrolyte diffusion rate differences in the pores with various sizes. It may also result from network connections between smaller and larger pores [60–62].

The high C_s of AC_{Chem} was partly due to its high *SSA* and microporous surface. This increased the number of areas available for electrolyte-ion storage within the numerous small pores. Other factors, such as conductivity, may also have had an influence, as described below. Compared with the C_{Pyrol} electrode in Figure S2, the AC_{Chem} electrode exhibited a much higher value.

The increased current density peak with a higher scan rate was due to higher ion mobility. This was associated with high concentrations that diffuse in close proximity to electrode surfaces [63,64].

Table 4. Summary of C_s values obtained at various scan rates for AC_{Chem} electrode compared to literature CW-based electrodes.

Scan Rate Setting (mV/s)	This Work C_s Values (F/g)	Literature C_s Values (F/g)
1	--	150 [65] 250 [39]
5	261	109 [32] 195 [39]
10	220	101 [32]
20	174	130 [65] 90 [32]
50	110	100 [65]
100	69	47 [32]
200	45	--

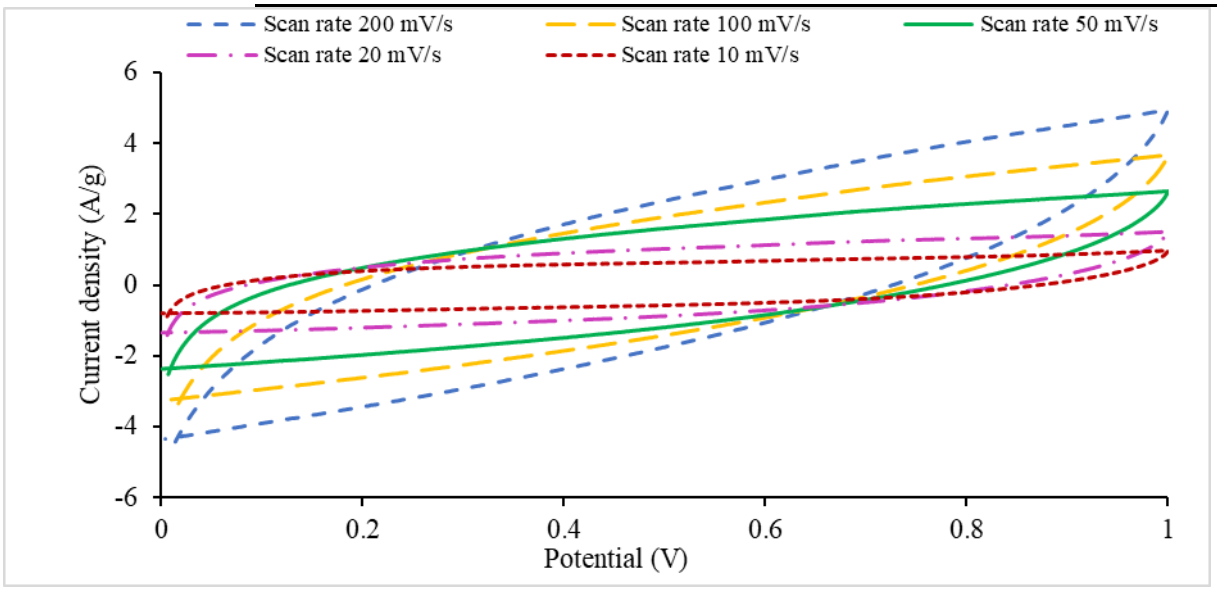

(**a**)

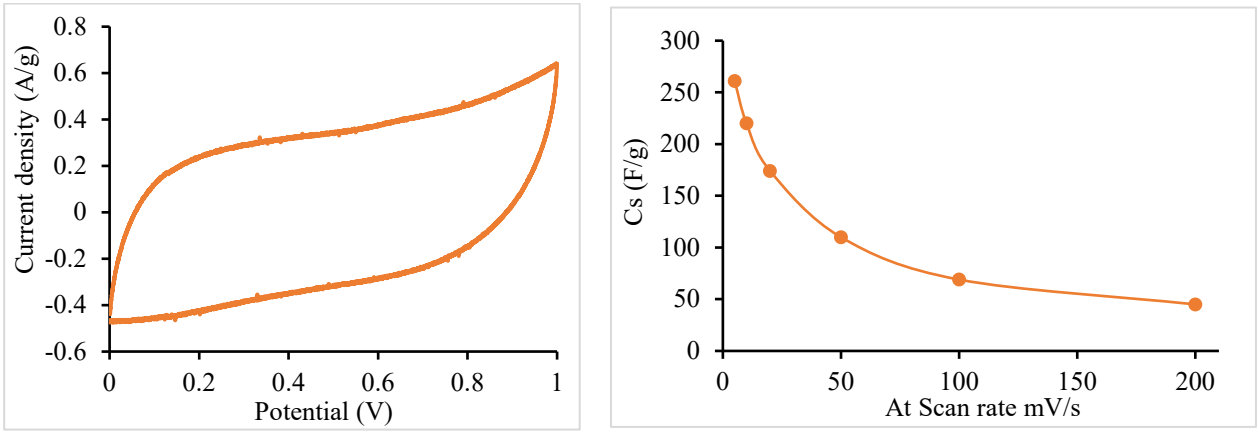

(**b**) (**c**)

Figure 6. CV studies on AC_{Chem} electrode. (**a**) At various scan rates; (**b**) at low scan rate (5 mV/s); (**c**) scan rate effect on C_s.

- ***GCD***

The supercapacitor performance can be further tested and verified by the GCD method (Figure 7). The AC_{Chem} electrode was charged and discharged galvostatically here, within a potential range of 0.0–1.0 V, at various constant discharge current density values (0.33, 0.67, 1.67, 3.3 and 5.0 A g^{-1}). These current density values were not arbitrarily chosen. Firstly, they spanned a variety of high and low values. At much higher values, the C_s normally become too small, while at much lower current density values, the C_s will increase unrealistically. Secondly, the chosen current density range was based on the current density values observed in CV plots of Figure 6, as extracted from Equation (2).

Figure 7a summarizes the potential (V) vs. time (s) plots, showing the charge and discharge processes. A potential drop (V_{IR}) was observed in the discharge after the maximum potential value was reached. From Figure 7a, the potential drops occurred in the discharge processes. The potential drop values were 0.064, 0.134, 0.297, 0.66 and 0.76 V at the above current density values, respectively. The C_s values from the GCD curves were estimated using Equation (3) [12], as summarized in Table 5.

$$C_s = \frac{(2 \times I)}{\left[\left(\frac{dV}{dt}\right) \times M\right]} = (2 \times I) \Big/ [(dV/dt) \times M] \quad (3)$$

where dv/dt is the slope for the linear-discharge curve, I is the discharge current (A) and M is the total mass (g) for the electrode.

The values for equivalent series resistance (ESR) from the GCD method, described in Table 5, can be evaluated by Equation (4). The ESR values were within a narrow domain, which confirmed the electrode stability at different densities. This is another superior feature of the present electrode.

$$ESR = V_{IR}/2I \quad (4)$$

Table 5. Characteristics for AC_{Chem} electrode measured at various discharge current values from GCD.

Discharge Current (A/g)	0.33	0.66	1.66	3.3	5.0
V_{IR} (V)	0.064	0.134	0.297	0.660	0.760
ESR (Ω)	3.20	3.35	3.00	3.30	2.53
C_s (F/g)	150	141	92	50	39

Charge and discharge processes were nearly symmetric, indicating high electrochemical reversibility for the electrode. The small V_{IR} drop in the discharging curves of

AC_{Chem} implied a small *ESR* value, which is an essential feature in supercapacitors with favorable power characteristics. The low V_{IR} drop in AC_{Chem} is due to its high conductivity, as achieved by $ZnCl_2$ activation. The C_s of AC_{Chem} decreased from 150 F/g (0.33 A/g) to 39 F/g (at 5 A/g), as shown in Figure 7b. This is a common supercapacitor behavior that is mainly due to electrolyte-ion diffusion limitations.

At higher currents, the time available for charging/discharging processes decreased due to higher ion mobility. This caused lower C_s, as expected, in congruence with the literature [8,55,66]. Figure 7a shows that at higher current density, a shorter time for charging and discharging was available. Thus, the voltage drop increased at a higher current density, corresponding to the resistance exhibited by the supercapacitor [12,67].

The specific energy and specific power values were calculated using Equations (5) and (6) [68,69].

$$E = \left[C_s \times \left(\Delta V_{op}\right)^2 \right] / (2 \times 3.6) \quad (5)$$

$$P = E \times 3600/\Delta t \quad (6)$$

where C_s value (F/g) is extracted from the discharge curve, ΔV_{op} is the operating voltage range (V) defined as $\Delta V_{op} = \Delta V_{appl} - V_{IR}$ and ΔV_{appl} (=1 V) is the applied voltage used during the charge–discharge process. Δt denotes discharge time (in s), and V_{IR} describes the voltage drop observed in the discharge plot caused by the immediate impact of the charge-to-discharge process transition.

Figure 7c displays the Ragone plot for the electrode. The maximum specific energy was (18.3 Wh/kg) at specific power (360 W/kg) at current density (0.33 A/g). At maximum specific power (1444 W/kg), the specific energy was (6.4 Wh/kg) at current density (1.66 A/g). These values are higher than the literature results for coffee waste electrodes. A recent report [32] showed a specific energy of 4.78 Wh/kg and a specific power of 137 W/kg at 1–5 A/g current densities. The present results confirmed the potential value of the AC_{Chem} electrode in future applications, as it combined high specific energy with high specific power together. Again, The AC_{Chem} electrode showed higher performance than the C_{Pyrol} (Figure S3).

The electrode stability on recycling is depicted in Figure 7d. The plot was constructed at a current density of 0.33 A/g for 5000 cycles and showed only a slight C_s lowering from 149 to 148 F/g. The results depicted the high electrode stability upon charge–discharge cycling, which is an important feature in supercapacitor technology.

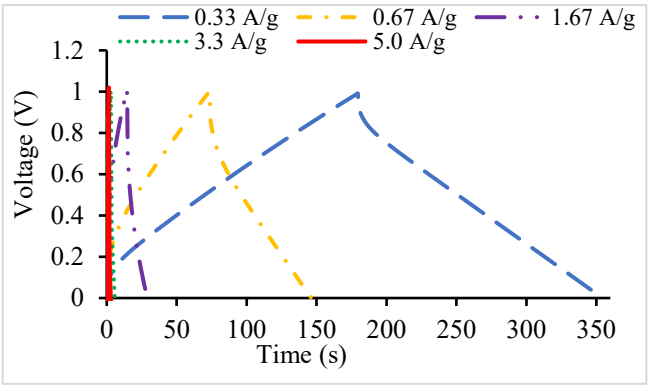

(**a**)

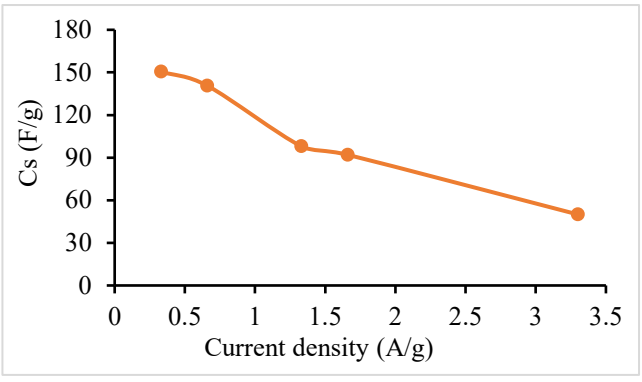

(**b**)

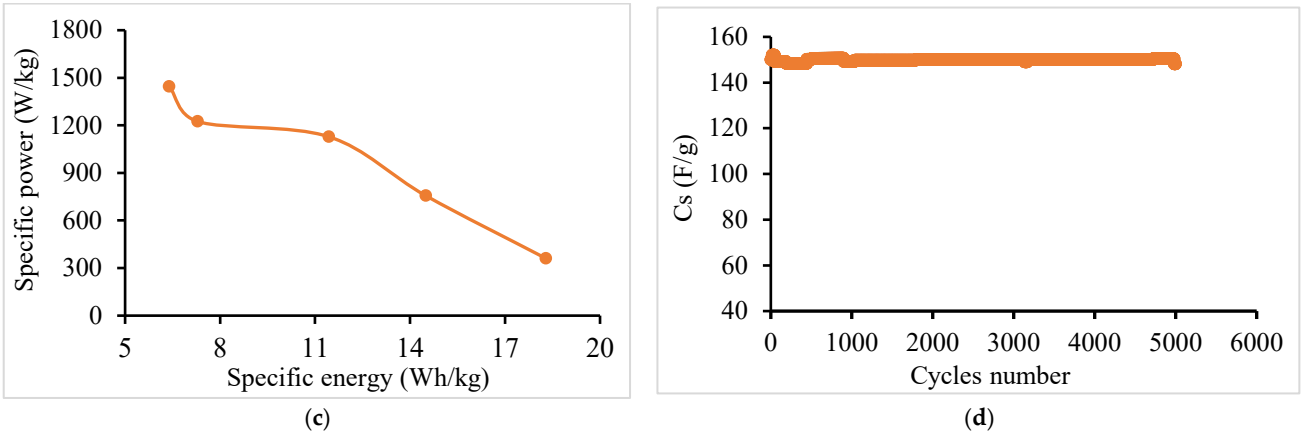

(**c**) (**d**)

Figure 7. GCD data for AC_{Chem} electrode. (**a**) Charge–discharge plots vs. time at different current density values. (**b**) Plots of C_s vs. current density. (**c**) The Ragone plot of specific power vs. specific energy. (**d**) Electrode stability with cycling (at 0.33 A/g).

- ***EIS***

To further confirm the above results, EIS was studied (Figure 8). Nyquist plots were constructed for the electrode within the frequency range (0.01–10 × 10^3 Hz) (Figure 8a). The *ESR* values indicated looseness inside the supercapacitor. The intercept with the *x*-axis, at a higher frequency, represented the combined resistance (Rs = 0.48 Ω) value involving electrode material inherent resistance, electrolyte solution ionic resistance and contact resistance at the current collector/electrode interface. The semicircle loop described electrode conductivity, together with its charge transfer resistance (R_{ct}) [70]. The measured R_{ct} here was 0.2 Ω. Higher electrode conductivity normally indicates a smaller semicircle loop. For AC_{Chem}, the calculated *ESR* ($R_s + R_{CT}$) here was 0.6 Ω. At low frequencies, the vertical line describes the electrode capacitive behaviors. In the present electrode, the Nyquist plot showed a nearly linear behavior, in parallel with the imaginary *y*-axis, indicating polarized systems. At low frequencies, deviation from vertical behavior to smaller slopes corresponded to higher ionic-diffusion resistance. AC_{Chem} EIS results were superior to the C_{Pyrol} electrode depicted in Supplementary Figure S4.

Time constants normally divide between the electrode capacitive and resistive regions. This can be determined from the reciprocal of maximum frequency (f_0) as $t_0 = 1/f_0$. Generally, a low time constant value indicates higher performance, i.e., a supercapacitor that yields a higher power in a shorter time. For the electrode, the knee frequency was 0.08 Hz, and the time constant was 12.5 s. Normally, the time constant value is affected by different factors, such as electrode material conductivity and thickness, together with electrolyte thickness [71]. When the electrode and electrolyte thicknesses are kept the same in the supercapacitors, then the time constant is influenced only by the electrode material conductivity.

Supercapacitor C_s values were calculated from EIS using the impedance imaginary component in Equation (7) [67,72].

$$C_s = 4 \times (-1/2\,\pi f z'' M) \quad (7)$$

where f denotes frequency (Hz), z'' is the impedance imaginary component (in Ω) and M is the mass of the electrode (in g).

Figure 8b shows how C_s varied with frequency. For the AC_{Chem} electrode, the C_s was 179 F/g at a frequency of 0.01 Hz.

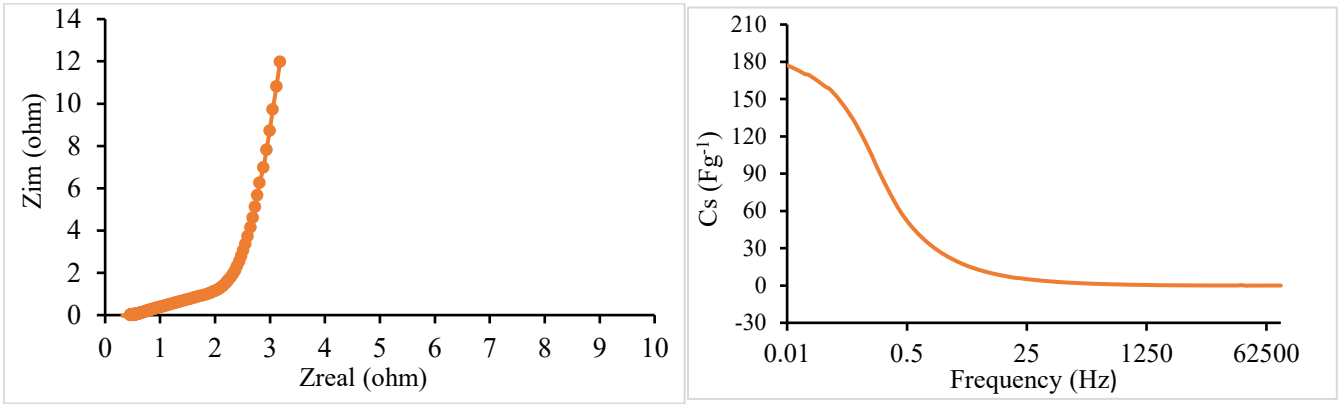

(**a**) (**b**)

Figure 8. *EIS* data measured for AC_{Chem} electrode. (**a**) Nyquist plot constructed. (**b**) C_s vs. frequency plot.

As described above, the C_s for the AC_{Chem} electrode was calculated by three methods. The CV study yielded a value of 261 F/g (at a scan rate of 5 mV/s), which is higher than the literature values for coffee waste electrodes. The GCD study yielded a value of 150 F/g at a discharge current of 0.01 A and *ESR* values in the range of 2.53–3.2 Ω at discharge currents in the range of 0.15–0.01 A. The EIS study showed a value of 179 F/g (at a frequency of 0.01 Hz) with low resistance. All values are superior to earlier reported values, as described above.

All in all, the results indicated that the AC_{Chem} electrode exhibited favorable physical characteristics, leading to improved supercapacitor performance. As described above, the chemical activating agent improved all characteristics of the activated carbon in many ways. The solid porosity was improved and yielded higher ion uptake. Graphitization and carbon purity were all improved. The relative crystallinity was improved, along with the electrical conductivity of AC. All these characteristics enabled the present AC_{Chem} electrode to exhibit high C_s and P_s at the same time. The present electrode here also exceeded earlier coffee waste-based electrodes, both in C_s and in P_s. One main factor was the careful protocol followed when preparing the AC_{Chem} electrode here. Material purity in terms of carbon content allowed the pores to uptake more ions with increased *Cs*. The carbon purity also allowed higher interparticle charge transfer in the electrode bulk, yielding lower resistance (~0.6 Ω here compared to ~10 Ω elsewhere), which was responsible for higher specific power. By combining high C_s and P_s together, the present electrode was also superior to many electrodes prepared from other biowastes and commercial carbons. This feature makes the electrode a potential candidate for future commercial supercapacitors. Therefore, it is necessary to examine new chemically activating agents that produce activated carbons from coffee and other biowastes. Research is active in these laboratories to further improve coffee waste-based ACs by other methods. Using natural electrolytes is being studied here to minimize environmental impact.

4. Conclusions

Two potentially useful carbon powders were produced from coffee wastes, one by pyrolysis under an inert atmosphere (C_{Pyrol}) with no added activators and the other with a $ZnCl_2$ activator (AC_{Chem}). The latter exhibited superior characteristics in terms of specific surface area, porosity, carbon content, graphitization and surface morphology. For these reasons, the AC_{Chem} electrode was given special attention in assessment as an electrode for supercapacitor purposes. Careful preparation procedures were followed to yield a high-purity carbon electrode that exhibited higher performance than earlier coffee waste-based electrodes in terms of specific capacitance and specific power. The electrode also exhibited low electrochemical series resistance with high stability. With these combined features, the new electrode competes with electrodes produced from other biowastes that showed

high performance in the literature. Using new types of chemical activators for coffee waste-based electrodes and using other preparation routes is recommended in future research.

Supplementary Materials: The following supporting information can be downloaded at https://www.mdpi.com/article/10.3390/pr12122832/s1.

Author Contributions: S.M.: Investigation, Writing—Original Draft. A.D.: Conceptualization, Supervision, Validation, Writing—Review and Editing, Validation. H.N.: Investigation, Supervision, Validation, Writing—Review and Editing. S.H.: Validation, Writing—Review and Editing. H.L.: Investigation (Characterization). H.H.: Investigation (Characterization). T.W.K.: Investigation (Characterization), Supervision, Validation. A.N.A.: Investigation (Characterization). H.S.H.: Supervision, Review Writing and Editing, Validation. All authors have read and agreed to the published version of the manuscript.

Funding: S.M. thanks An-Najah National University for the "thesis funding policy". T.W.K. acknowledges and thanks "the National Research Council of Science & Technology (NST) grant from the Korean government (MSIT) (# CAP20034-200)". No special fund was available for this project.

Data Availability Statement: All relevant data will be made available upon request.

Acknowledgments: Results are mostly based on S.M.'s PhD thesis. Help from the technical staff at An-Najah National University laboratories is acknowledged.

Conflicts of Interest: The work carries no conflicts of interest.

References

1. Huang, H.; Wang, X. Graphene nanoplate-MnO_2 composites for supercapacitors: A controllable oxidation approach. *Nanoscale* **2011**, *3*, 3185–3191.
2. Cheng, Q.; Tang, J.; Ma, J.; Zhang, H.; Shinya, N.; Qin, L.-C. Graphene and nanostructured MnO_2 composite electrodes for supercapacitors. *Carbon* **2011**, *49*, 2917–2925.
3. Yang, H. Graphene-Based Supercapacitor for Energy Storage Applications. Master's Thesis, The Ohio State University, Columbus, OH, USA, 2013.
4. Singh, A.; Roberts, A.J.; Slade, R.C.T.; Chandra, A. High electrochemical performance in asymmetric supercapasitors using MWCNT/nickel sulfide composite and graphene nanoplates as electrodes. *J. Mater. Chem. A* **2014**, *2*, 16723–16730.
5. Libich, J.; Máca, J.; Vondrák, J.; Čech, O.; Sedlaříková, M. Supercapacitors: Properties and applications. *J. Energy Storage* **2018**, *17*, 224–227.
6. Vangari, M.; Pryor, T.; Jiang, L. Supercapacitors: Review of materials and fabrication methods. *J. Energy Eng.* **2013**, *139*, 72–79.
7. Lufrano, F.; Staiti, P. Mesoporous carbon materials as electrodes for electrochemical supercapacitors. *Int. J. Electrochem. Sci.* **2010**, *5*, 903–916.
8. Lu, M. Graphene-Based Materials for Supercapacitor Electrodes. Ph.D. Theses, National University of Singapore, Singapore, 2013.
9. Kötz, R.; Carlen, M. Principles and applications of electrochemical capacitors. *Electrochim. Acta* **2000**, *45*, 2483–2498.
10. Guo, Q.; Zhou, X.; Li, X.; Chen, S.; Seema, A.; Greiner, A.; Hou, H. Supercapacitors based on hybrid carbon nanofibers containing multiwalled carbon nanotubes. *J. Mater. Chem.* **2009**, *19*, 2810–2816.
11. Stoller, M.D.; Ruoff, R.S. Best practice methods for determining an electrode material's performance for Ultracapacitors. *J. Energy Environ. Sci.* **2010**, *3*, 1294–1301.
12. Basri, N.H.; Dolah, B.N.M.; Farma, R.; Deraman, M.; Awitdrus Talib, I.A.; Omar, R.; Manjunatha, J.G.; Ishak, M.M. Physical and electrochemical properties of supercapacitor electrodes derived from carbon nanotube and biomass carbon. *Int. J. Electrochem. Sci.* **2013**, *8*, 257–273.
13. Li, W.; Peng, J.; Zhang, L.; Yang, K.; Xia, H.; Zhang, S.; Guo, S.-H. Preparation of activated carbon from coconut shell chars in pilot-scale microwave heating equipment at 60 kW. *Waste Manag.* **2009**, *29*, 756–760.
14. Arrebola, J.; Caballero, A.; Hernán, L.; Morales, J.; Olivares-Marín, M.; Gómez-Serrano, V. Improving the performance of biomass-derived carbons in Li-ion batteries by controlling the lithium insertion process. *J. Electrochem. Soc.* **2010**, *157*, A791.
15. Kalyani, P.; Anitha, A.; Darchen, A. Obtaining Activated Carbon from Papaya Seeds for Energy Storage Devices. *Int. J. Eng. Sci. Res. Technol.* **2015**, *4*, 110–122.
16. Li, W.; Zhang, L.-B.; Peng, J.-H.; Li, N.; Zhu, X.-Y. Preparation Of High Surface Area Activated Carbons From Tobacco Stems With K2CO3 Activation Using Microwave Radiation. *Ind. Crops Prod.* **2008**, *27*, 341–347.
17. Hesas, R.H.; Daud, W.M.A.W.; Sahu, J.; Arami-Niya, A. The Effects of A Microwave Heating Method on The Production of Activated Carbon from Agricultural Waste: A Review. *J. Anal. Appl. Pyrolysis* **2021**, *100*, 1–11.

18. Yang, K.; Peng, J.; Srinivasakannan, C.; Zhang, L.; Xia, H.; Duan, X. Preparation Of High Surface Area Activated Carbon From Coconut Shells Using Microwave Heating. *Bioresour. Technol.* **2010**, *101*, 6163–6169.
19. Hwang, J.Y.; Li, M.; El-Kady, M.F.; Kaner, R.B. Next-generation activated carbon supercapacitors: A simple step in electrode processing leads to remarkable gains in energy density. *Adv. Funct. Mater.* **2017**, *27*, 1605745.
20. Jiang, L.; Yan, J.; Hao, L.; Xue, R.; Sun, G.; Yi, B. High rate performance activated carbons prepared from ginkgo shells for electrochemical supercapacitors. *Carbon* **2013**, *56*, 146–154.
21. Hong, P.; Liu, X.; Zhang, X.; Peng, S.; Zou, T.; Wang, Z.; Yang, Y.; Zhao, R.; Chen, Y.; Wang, Y. Potassium sulphate (K_2SO_4) activation of chestnut shell to oxygen-enriched porous carbons with enhanced capacitive properties. *Int. J. Energy Res.* **2020**, *44*, 5385–5396.
22. Cheng, L.; Guo, P.; Wang, R.; Ming, L.; Leng, F.; Li, H.; Zhao, X. Electrocapacitive properties of supercapacitors based on hierarchical porous carbons from chestnut shell. *Colloids Surf. A Physicochem. Eng. Asp.* **2014**, *446*, 127–133.
23. Wan, L.; Li, X.; Li, N.; Xie, M.; Du, C.; Zhang, Y.; Chen, J. Multi-heteroatom-doped hierarchical porous carbon derived from chestnut shell with superior performance in supercapacitors. *J. Alloys Compd.* **2019**, *790*, 760–771.
24. Czerwinska, N.; Giosuè, C.; Matos, I.; Sabbatini, S.; Ruello, M.L.; Bernardo, M. Development of activated carbons derived from wastes: Coffee grounds and olive stones as potential porous materials for air depollution. *Sci. Total Environ.* **2024**, *914*, 169898.
25. Pagett, M.; Teng, K.S.; Sullivan, G.; Zhang, W. Reusing waste coffee grounds as electrode materials: Recent advances and future opportunities. *Glob. Chall.* **2023**, *7*, 2200093.
26. Aouay, F.; Attia, A.; Dammak, L.; Ben Amar, R.; Deratani, A. Activated carbon prepared from waste coffee grounds: Characterization and adsorption properties of dyes. *Materials* **2024**, *17*, 3078.
27. AlMarzooqi, A.; Almazrouei, H.; Alhammadi, H. Drugs Removal from Wastewater with Activated Carbon from Coffee Waste. *Int. J. Biomed. Res. Pract.* **2024**, *4*, 1–5.
28. Kim, C.-H.; Lee, S.-Y.; Park, S.-J. Valorization of waste coffee grounds into microporous carbon materials for CO_2 adsorption. *Green Chem.* **2024**, *26*, 1901–1909.
29. Pandey, K.; Jeong, H.K. Coffee waste-derived porous carbon based flexible supercapacitors. *Chem. Phys. Lett.* **2022**, *809*, 140173.
30. Chiu, Y.-H.; Lin, L.-Y. Effect of activating agents for producing activated carbon using a facile one-step synthesis with waste coffee grounds for symmetric supercapacitors. *J. Taiwan Inst. Chem. Eng.* **2019**, *101*, 177–185.
31. Biegun, M.; Dymerska, A.; Chen, X.; Mijowska, E. Study of the active carbon from used coffee grounds as the active material for a high-temperature stable supercapacitor with ionic-liquid electrolyte. *Materials* **2020**, *13*, 3919.
32. Khadka, O.; Lawaju, U.; Koju, S.; Rai, R.C.; Nakarmi, M.L.; Joshi, P. Activated carbon derived from coffee waste as supercapacitor electrode material. *Sci. World* **2024**, *17*, 19–26.
33. Davidraj, J.M.; Sathish, C.I.; Benzigar, M.R.; Li, Z.; Zhang, X.; Bahadur, R.; Ramadass, K.; Singh, G.; Yi, J.; Kumar, P. Recent advances in food waste-derived nanoporous carbon for energy storage. *Sci. Technol. Adv. Mater.* **2024**, *25*, 2357062.
34. Rufford, T.E.; Hulicova-Jurcakova, D.; Zhu, Z.; Lu, G.Q. Nanoporous carbon electrode from waste coffee beans for high performance supercapacitors. *Electrochem. Commun.* **2008**, *10*, 1594–1597.
35. Borghei, S.A.; Zare, M.H.; Ahmadi, M.; Sadeghi, M.H.; Marjani, A.; Shirazian, S.; Ghadiri, M. Synthesis of multi-application activated carbon from oak seeds by KOH activation for methylene blue adsorption and electrochemical supercapacitor electrode. *Arab. J. Chem.* **2021**, *14*, 102958.
36. Said, B.; Bacha, O.; Rahmani, Y.; Harfouche, N.; Kheniche, H.; Zerrouki, D.; Belkhalfa, H.; Henni, A. Activated carbon prepared by hydrothermal pretreatment-assisted chemical activation of date seeds for supercapacitor application. *Inorg. Chem. Commun.* **2023**, *155*, 111012.
37. Zyoud, A.; Nassar, H.N.; El-Hamouz, A.; Hilal, H.S. Solid olive waste in environmental cleanup: Enhanced nitrite ion removal by ZnCl2-activated carbon. *J. Environ. Manag.* **2015**, *152*, 27–35.
38. Rufford, T.E.; Hulicova-Jurcakova, D.; Fiset, E.; Zhu, Z.; Lu, G.Q. Double-layer capacitance of waste coffee ground activated carbons in an organic electrolyte. *Electrochem. Commun.* **2009**, *11*, 974–977.
39. Farma, R.; Julita, R.I.; Apriyani, I.; Awitdrus, A.; Taer, E. ZnCl2-assisted synthesis of coffee bean bagasse-based activated carbon as a stable material for high-performance supercapacitors. *Mater. Today Proc.* **2023**, *87*, 25–31.
40. Williams, P.T.; Reed, A.R. Development of activated carbon pore structure via physical and chemical activation of biomass fibre waste. *Biomass Bioenergy* **2006**, *30*, 144–152.
41. Le Van, K.; Luong Thi Thu, T. Preparation of Pore-Size Controllable Activated Carbon from Rice Husk Using Dual Activating Agent and Its Application in Supercapacitor. *J. Chem.* **2019**, *2019*, 4329609.
42. Ruiz, S.; Tamayo, J.A.; Delgado Ospina, J.; Navia Porras, D.P.; Valencia Zapata, M.E.; Mina Hernandez, J.H.; Valencia, C.H.; Zuluaga, F.; Grande Tovar, C.D. Antimicrobial films based on nanocomposites of chitosan/poly(vinyl alcohol)/graphene oxide for biomedical applications. *Biomolecules* **2019**, *9*, 109.
43. Lowell, S.; Shields, J.E.; Thomas, M.A.; Thommes, M. *Characterization of Porous Solids and Powders: Surface Area, Pore Size and Density*; Springer Science & Business Media: New York, NY, USA, 2012; Volume 16.
44. Puziy, A.; Poddubnaya, O.; Martınez-Alonso, A.; Suárez-Garcıa, F.; Tascón, J. Synthetic carbons activated with phosphoric acid: I. Surface chemistry and ion binding properties. *Carbon* **2002**, *40*, 1493–1505.
45. Islam, M.S.; Ang, B.C.; Gharehkhani, S.; Afifi, A.B.M. Adsorption capability of activated carbon synthesized from coconut shell. *Carbon Lett.* **2016**, *20*, 1–9.

46. Gao, Y.; Shi, W.; Wang, W.; Wang, Y.; Zhao, Y.; Lei, Z.; Miao, R. Ultrasonic-assisted production of graphene with high yield in supercritical CO2 and its high electrical conductivity film. *Ind. Eng. Chem. Res.* **2014**, *53*, 2839–2845.
47. Anastacio-López, Z.S.; Gonzalez-Calderon, J.; Saldivar-Guerrero, R.; Velasco-Santos, C.; Martínez-Hernández, A.L.; Fierro-González, J.C.; Almendárez-Camarillo, A. Modification of graphene oxide to induce beta crystals in isotactic polypropylene. *J. Mater. Sci.* **2019**, *54*, 427–443.
48. Abbas, M.; Kaddour, S.; Trari, M. Kinetic and equilibrium studies of cobalt adsorption on apricot stone activated carbon. *J. Ind. Eng. Chem.* **2014**, *20*, 745–751.
49. Liu, Y.; Liu, X.; Dong, W.; Zhang, L.; Kong, Q.; Wang, W. Efficient adsorption of sulfamethazine onto modified activated carbon: A plausible adsorption mechanism. *Sci. Rep.* **2017**, *7*, 12437.
50. Gupta, G.K.; Sagar, P.; Pandey, S.K.; Srivastava, M.; Singh, A.; Singh, J.; Srivastava, A.; Srivastava, S.; Srivastava, A. In situ fabrication of activated carbon from a bio-waste desmostachya bipinnata for the improved supercapacitor performance. *Nanoscale Res. Lett.* **2021**, *16*, 85.
51. Gupta, A.; Dhakate, S.R.; Pal, P.; Dey, A.; Iyer, P.K.; Singh, D.K. Effect of graphitization temperature on structure and electrical conductivity of poly-acrylonitrile based carbon fibers. *Diam. Relat. Mater.* **2017**, *78*, 31–38.
52. Hernández-Montoya, V.; García-Servin, J.; Bueno-López, J.I. Thermal treatments and activation procedures used in the preparation of activated carbons. In *Lignocellulosic Precursors Used in the Synthesis of Activated Carbon-Characterization Techniques and Applications in the Wastewater Treatment*; Intech: Rijeka, Croatia, 2012; pp. 19–36.
53. Bergna, D.; Varila, T.; Romar, H.; Lassi, U. Comparison of the properties of activated carbons produced in one-stage and two-stage processes. *C* **2018**, *4*, 41.
54. Mohamedkhair, A.K.; Aziz, M.A.; Shah, S.S.; Shaikh, M.N.; Jamil, A.K.; Qasem, M.A.A.; Buliyaminu, I.A.; Yamani, Z.H. Effect of an activating agent on the physicochemical properties and supercapacitor performance of naturally nitrogen-enriched carbon derived from Albizia procera leaves. *Arab. J. Chem.* **2020**, *13*, 6161–6173.
55. Daraghmeh, A.; Hussain, S.; Servera, L.; Xuriguera, E.; Blanes, M.; Ramos, F.; Cornet, A.; Cirera, A. Flexible supercapacitors based on low-cost tape casting of high dense carbon nanofibers. *Mater. Res. Express* **2017**, *4*, 025007.
56. Kim, S.Y.; Noh, Y.J.; Yu, J. Thermal conductivity of graphene nanoplatelets filled composites fabricated by solvent-free processing for the excellent filler dispersion and a theoretical approach for the composites containing the geometrized fillers. *Compos. Part A Appl. Sci. Manuf.* **2015**, *69*, 219–225.
57. Jarrar, S.; Hussain, S.; Haq, A.U.; Bhattacharya, G.; Saadeddin, I.; Servera, L.; Ruiz, J.; Janem, A.; Daraghmeh, A. Binder-free all-carbon composite supercapacitors. *Nanotechnology* **2024**, *35*, 305708.
58. Prabaharan, S.; Vimala, R.; Zainal, Z. Nanostructured mesoporous carbon as electrodes for supercapacitors. *J. Power Sources* **2006**, *161*, 730–736.
59. Saha, D.; Li, Y.; Bi, Z.; Chen, J.; Keum, J.K.; Hensley, D.K.; Grappe, H.A.; Meyer III, H.M.; Dai, S.; Paranthaman, M.P. Studies on supercapacitor electrode material from activated lignin-derived mesoporous carbon. *Langmuir* **2014**, *30*, 900–910.
60. Frackowiak, E.; Beguin, F. Carbon materials for the electrochemical storage of energy in capacitors. *Carbon* **2001**, *39*, 937–950.
61. Lim, C.-S.; Teoh, K.; Liew, C.-W.; Ramesh, S. Electric double layer capacitor based on activated carbon electrode and biodegradable composite polymer electrolyte. *Ionics* **2014**, *20*, 251–258.
62. Meher, S.K.; Justin, P.; Ranga Rao, G. Microwave-mediated synthesis for improved morphology and pseudocapacitance performance of nickel oxide. *ACS Appl. Mater. Interfaces* **2011**, *3*, 2063–2073.
63. Graydon, J.W.; Panjehshahi, M.; Kirk, D.W. Charge redistribution and ionic mobility in the micropores of supercapacitors. *J. Power Sources* **2014**, *245*, 822–829.
64. Jayawickramage, R.A.P.; Ferraris, J.P. High performance supercapacitors using lignin based electrospun carbon nanofiber electrodes in ionic liquid electrolytes. *Nanotechnology* **2019**, *30*, 155402.
65. Choi, J.; Zequine, C.; Bhoyate, S.; Lin, W.; Li, X.; Kahol, P.; Gupta, R. Waste coffee management: Deriving high-performance supercapacitors using nitrogen-doped coffee-derived carbon. *C* **2019**, *5*, 44.
66. Jarrar, S. Carbon Nanofibers/Graphene Nanoplateletes Composite as Supercapacitor Electrode Using KOH Aqueous Electrolyte. Master's Thesis, An-Najah National University, Nablus, Palestine, 2020.
67. Daraghmeh, A.; Hussain, S.; Servera, L.; Xuriguera, E.; Cornet, A.; Cirera, A. Impact of binder concentration and pressure on performance of symmetric CNFs based supercapacitors. *Electrochim. Acta* **2017**, *245*, 531–538.
68. Zhou, Y.; Jin, P.; Zhou, Y.; Zhu, Y. High-performance symmetric supercapacitors based on carbon nanotube/graphite nanofiber nanocomposites. *Sci. Rep.* **2018**, *8*, 9005.
69. Ganesh, V.; Pitchumani, S.; Lakshminarayanan, V. New symmetric and asymmetric supercapacitors based on high surface area porous nickel and activated carbon. *J. Power Sources* **2006**, *158*, 1523–1532.

70. Gong, Y.; Li, D.; Fu, Q.; Pan, C. Influence of graphene microstructures on electrochemical performance for supercapacitors. *Prog. Nat. Sci. Mater. Int.* **2015**, *25*, 379–385.
71. Schütter, C.; Ramirez-Castro, C.; Oljaca, M.; Passerini, S.; Winter, M.; Balducci, A. Activated carbon, carbon blacks and graphene based nanoplatelets as active materials for electrochemical double layer capacitors: A comparative study. *J. Electrochem. Soc.* **2014**, *162*, A44.
72. Calvo, E.; Lufrano, F.; Staiti, P.; Brigandì, A.; Arenillas, A.; Menéndez, J. Optimizing the electrochemical performance of aqueous symmetric supercapacitors based on an activated carbon xerogel. *J. Power Sources* **2013**, *241*, 776–782.